A Model for Neural Development and Treatment of Rett Syndrome Using Human Induced Pluripotent Stem Cells

Maria C.N. Marchetto,[1,5] Cassiano Carromeu,[2,5] Allan Acab,[2] Diana Yu,[1] Gene W. Yeo,[3] Yangling Mu,[1] Gong Chen,[4] Fred H. Gage,[1] and Alysson R. Muotri[2,*]

[1]The Salk Institute for Biological Studies, 10010 North Torrey Pines Road, La Jolla, CA 92037, USA
[2]University of California San Diego, School of Medicine, Department of Pediatrics, Rady Children's Hospital San Diego, Department of Cellular and Molecular Medicine, Stem Cell Program, 9500 Gilman Drive, La Jolla, CA 92093, USA
[3]University of California San Diego, School of Medicine, Department of Cellular & Molecular Medicine, Stem Cell Program, 9500 Gilman Drive, La Jolla, CA 92093, USA
[4]Pennylvania State University, Department of Biology. 201 Life Science Building, University Park, PA 6802, USA
[5]These authors contributed equally to the work
*Correspondence: muotri@ucsd.edu
DOI 10.1016/j.cell.2010.10.016

SUMMARY

Autism spectrum disorders (ASD) are complex neurodevelopmental diseases in which different combinations of genetic mutations may contribute to the phenotype. Using Rett syndrome (RTT) as an ASD genetic model, we developed a culture system using induced pluripotent stem cells (iPSCs) from RTT patients' fibroblasts. RTT patients' iPSCs are able to undergo X-inactivation and generate functional neurons. Neurons derived from RTT-iPSCs had fewer synapses, reduced spine density, smaller soma size, altered calcium signaling and electrophysiological defects when compared to controls. Our data uncovered early alterations in developing human RTT neurons. Finally, we used RTT neurons to test the effects of drugs in rescuing synaptic defects. Our data provide evidence of an unexplored developmental window, before disease onset, in RTT syndrome where potential therapies could be successfully employed. Our model recapitulates early stages of a human neurodevelopmental disease and represents a promising cellular tool for drug screening, diagnosis and personalized treatment.

INTRODUCTION

Autism spectrum disorders (ASD) are complex neurodevelopmental diseases affecting 1 in 150 children in the United States (Autism and Developmental Disabilities Monitoring Network Surveillance Year 2000 Prinicipal Investigators; Centers for Disease Control and Prevention, 2007). Such diseases are mainly characterized by impaired social interaction and repetitive behavior. Family history and twin studies suggest that, in some cases, these disorders share genetic roots, but the degree to which environmental and genetic patterns account for individual differences within ASD is currently unknown (Piven et al., 1997; Ronald et al., 2006). A different combination of genetic mutations is likely to play a role in each individual. Nevertheless, the study of mutations in specific genes can help to identify molecular mechanisms responsible for subtle alterations in the nervous system, perhaps pointing to common mechanisms for ASD.

Rett syndrome (RTT) is a progressive neurological disorder caused by mutations in the X-linked gene encoding MeCP2 protein (Amir et al., 1999). RTT patients have a large spectrum of autistic characteristics and are considered part of the ASD population (Hammer et al., 2002; Samaco et al., 2005, 2004; Zappella et al., 2003). These individuals undergo apparently normal development until 6–18 months of age, followed by impaired motor function, stagnation and then regression of developmental skills, hypotonia, seizures and autistic behavior (Amir et al., 1999). MeCP2 may be involved in the epigenetic regulation of target genes, by binding to methylated CpG dinucleotides within promoters, and may function as a transcriptional repressor, although this view has been challenged recently (Chahrour et al., 2008; Yasui et al., 2007).

Pluripotent human embryonic stem cells (hESCs) have been successfully generated from early stage human embryos and can differentiate into various cell types (Thomson et al., 1998). However, to develop cellular models of human disease, it is necessary to generate cell lines with genomes predisposed to diseases. Recently, reprogramming of somatic cells to a pluripotent state by overexpression of specific genes (induced pluripotent stem cells, iPSCs) has been accomplished (Takahashi and Yamanaka, 2006; Yu et al., 2007). Isogenic pluripotent cells are attractive not only for their potential therapeutic use with lower risk of immune rejection but also for understanding complex diseases (Marchetto et al., 2010; Muotri, 2008). Although iPSCs have been generated for several neurological diseases (Dimos et al., 2008; Ebert et al., 2009; Hotta et al., 2009; Lee et al., 2009; Park et al., 2008; Soldner et al., 2009), the demonstration

of disease-specific pathogenesis and phenotypic rescue in relevant cell types is a current challenge in the field (Marchetto et al., 2010).

We have developed a human model of RTT by generating iPSCs from fibroblasts of RTT patients carrying different MeCP2 mutations and unaffected individuals. We show that RTT-iPSCs retained the capacity to generate proliferating neural progenitor cells (NPCs) and functional neurons that underwent X-inactivation. We observed a reduced number of dendritic spines and synapses in iPSC-derived neurons. Moreover, we detected an altered frequency of intracellular calcium spikes and electrophysiological defects in RTT-derived neuronal networks, revealing potential new biomarkers for RTT pathology. Gain and loss of function experiments in iPSC-derived neurons confirmed that some of the alterations observed were related to MeCP2 expression levels. Finally, we used the iPSC system to test candidate drugs to rescue synaptic deficiency in RTT neurons. Together, our results suggest that RTT and other complex CNS diseases can be modeled using the iPSC technology to investigate the cellular and molecular mechanisms underlying their abnormalities.

RESULTS

Generation of iPSCs from RTT Patients and Normal Individuals

Nonaffected control fibroblasts and cells carrying four distinct MeCP2 mutations (Figure 1A and Table S1 available online) isolated from clinically affected female patients with RTT symptoms were infected with retroviral reprogramming vectors (Sox2, Oct4, c-Myc and Klf4), as described elsewhere (Takahashi et al., 2007). After 2 to 3 weeks, compact iPSC colonies emerged from a background of fibroblasts (Figures 1B and 1C). Colonies were manually picked and transferred to matrigel (Figures 1D and 1E). We obtained at least 10 clones from each control (WT)-iPSC and RTT-iPSC that continuously expressed pluripotent markers such as Nanog, Lin28, Tra-1-81 and Sox2 (Figures 1F and 1G and Figures S1A–S1C). All iPSC clones used in this study maintained a normal karyotype (Figure 1H). Teratomas containing derivatives from all 3 embryonic germ layers confirmed that the iPSCs were able to differentiate in vivo (Figure 1I). PCR fingerprinting confirmed their derivation from respective fibroblasts (data not shown). Next, we asked if the global molecular signatures of RTT-iPSC clones carrying the two distinct MeCP2 mutations (1155del32 and Q244X) and WT-iPSC clones (from AG09319) resembled those of available hESC lines (HUES6). Gene expression profiles measured using human genome Affymetrix Gene Chip arrays were grouped by hierarchical clustering, and correlation coefficients were computed for all pair-wise comparisons (GEO accession number GSE21037). We observed that the WT-iPSC and RTT-iPSC clones were almost indistinguishable. The results clearly revealed that the iPSC and hESC lines were more similar to each other than to the respective original fibroblasts (Figure S1D). These findings, combined with manual inspection of the gene expression of known pluripotent- and fibroblast-related genes (Figures S1E and S1F), indicated that the reprogramming was

successful. In Table S2 we present a summary of all iPSC subjects and clones utilized for each experiment.

Neural Induction of iPSCs

Our protocol for neuronal differentiation is outlined in Figure 2A. We initiated neural differentiation by plating embryoid bodies (EBs). After a week, EB-derived rosettes became apparent (Figure 2B). Rosettes were then manually collected, dissociated and re-plated. The NPCs derived from rosettes formed a homogeneous population after a couple of passages. NPCs were positive for early neural precursor markers, such as Nestin, Sox1-2 and Musashi1 (Figure 2C). To obtain mature neurons, EBs in the presence of retinoic acid (RA) were dissociated and re-plated (Figure 2B). At this stage, cells were positive for Tuj1 (β-III-Tubulin) and Map2 (Microtubule-associated protein 2) (Figure 2D). Moreover, we detected expression of GABA (γ-amino butyric acid) and VGLUT1 (vesicular glutamate transporter-1). We also observed synapsin puncta outlining Map2-positive neurites (Figure 2D). We did not detect a significant alteration in RTT neuronal survival when compared to controls, as measured by Map2 staining (Figure 2E and Figure S2A). In addition, infection with a lentivirus expressing the *DsRed* gene under the control of *Synapsin* promoter (Syn::DsRed) did not reveal any difference in neuronal survival between RTT and controls (Figure 2E and Figure S2B). Interestingly, the number of GABA-positive neurons was also not affected between RTT and controls (Figure 2F and Figure S2C).

X-Inactivation during Neuronal Differentiation of RTT-iPSCs

In female hESCs, both chromosomes should be active, but one X chromosome becomes silenced upon differentiation (Dhara and Benvenisty, 2004). Similar to ESCs, female mouse iPSCs have shown reactivation of a somatically silenced X chromosome and have undergone random X-inactivation upon differentiation (Maherali et al., 2007). Because MeCP2 is an X-linked gene, we examined the ability of our RTT-iPSCs clones to reset the X chromosome (i.e., to erase X-inactivation) and whether X-inactivation would take place again after neuronal differentiation (Figure 3A). We stained RTT-iPSCs clones and their respective fibroblasts with an antibody against trimethylated histone 3 Lysine 27 (me3H3K27), an epigenetic silencing marker present on the inactive X chromosome in interphase nuclei (Silva et al., 2003). Some, but not all, undifferentiated RTT-iPSCs clones displayed diffuse immunoreactivity throughout the nucleus, similar to some hESCs, showing that the memory of the previous inactivation state had been erased (Figure 3B). For further analysis, we only selected clones that displayed a diffuse me3H3K27 pattern to differentiate into neurons. Upon neuronal differentiation, intense nuclear foci staining, a prominent diagnostic of the inactive X, was found in 80% of neurons labeled by the infection of a lentivirus carrying the neuron-specific *Synapsin* promoter driving the EGFP reporter (Syn::EGFP). Nuclear foci were also present in RTT fibroblasts before reprogramming (Figure 3B). We quantified the percentage of cells displaying either a diffuse or intense X-inactivation (nuclear foci) (Figure 3C). Our data suggest that the majority of cells in selected clones from both hESCs (99%) and iPSCs (95%) have a diffuse pattern. In contrast,
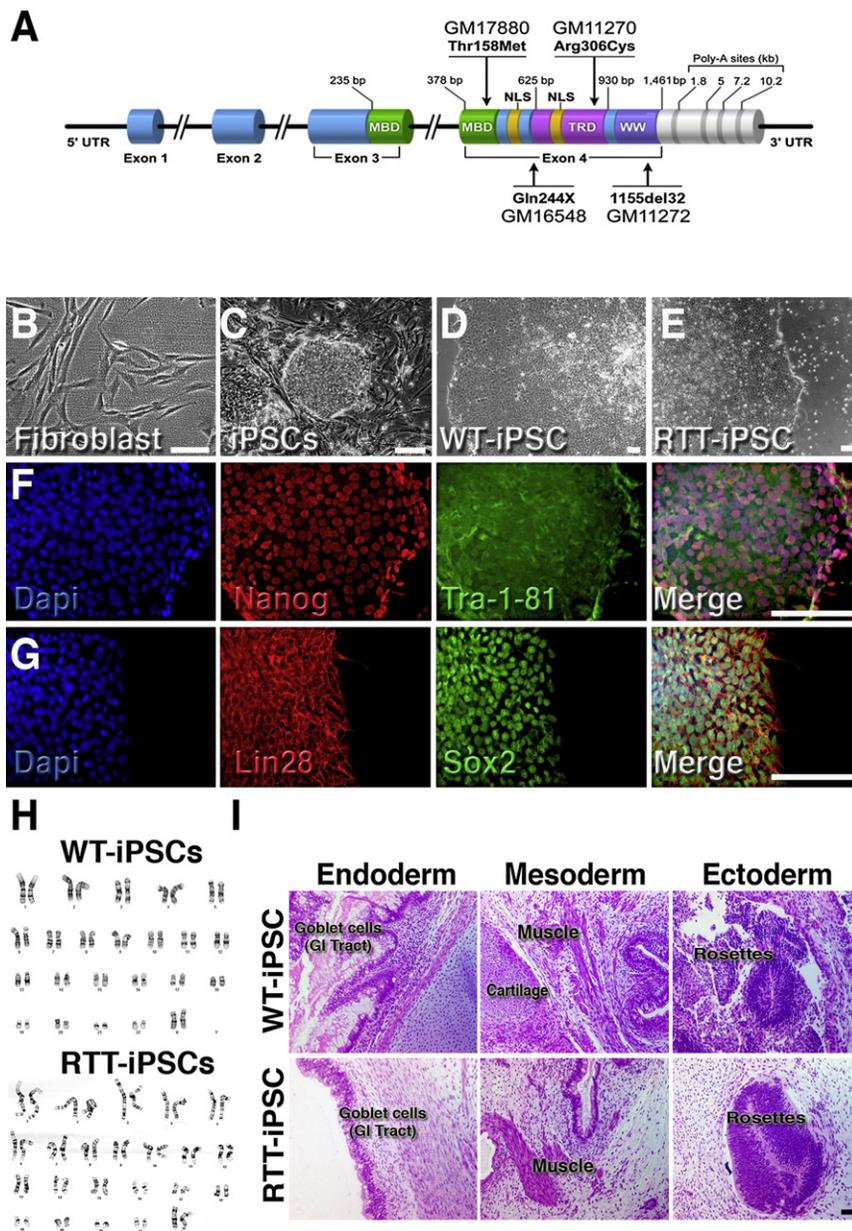
Figure 1. Generation of iPSCs

(A) Schematic representation of the MeCP2 gene structure and mutations used in this study. UTR, untranslated region; MBD, methyl-CpG binding domain; NLS, nuclear localization signal; Poly-A, polyadenylation signal; TRD, transcriptional repression domain; WW, domain-containing WW; X, stop codon. Respective cell-line codes are shown close to their mutations.

(B) Morphology of human fibroblasts before retroviral infection.

(C) Aspect of iPSCs colonies 14 days after infection.

(D and E) Representative images of established iPSC colonies.

(F and G) Representative images of RTT-iPSCs showing expression of pluripotent markers.

(H) No karyotypic abnormalities were observed.

(I) Representative images of teratoma sections.

The scale bar represents 100 μm.

See also Figure S1.

chromosomes (Figure 3E). As a consequence of both X-chromosomes' activation after reprogramming, the MeCP2 protein can be detected in undifferentiated iPSCs from RTT patients (Figure 3F). However, after differentiation, RTT-iPSC-derived neurons recapitulated X-inactivation and the population became mosaic regarding MeCP2 expression. Immunostaining was performed on several RTT-iPSC clones, and a representative example of MeCP2 expression after differentiation is shown in Figure 3F. Clones obtained from RTT fibroblasts carrying the 1155del32 MeCP2 mutation do not produce a full-length MeCP2 protein (Traynor et al., 2002). Next, we selected one WT-iPSC clone (WT-33 C1) and one RTT-iPSC clone (1155del32 C15) to determine whether the RTT-iPSC-derived neuronal population showed reduced MeCP2 protein levels. As expected, we observed a reduction in the full-length MeCP2 protein amounts in both fibroblasts and neurons derived from the RTT-iPSC clone (Figure 3G). We tested the original fibroblasts and iPSC-derived neurons from this patient for X-inactivation using standard methodology for the androgen receptor locus (Allen et al., 1992). RTT fibroblasts carrying the 1155del32 MeCP2 mutation had a 55:45 distribution, but RTT-derived neurons showed highly skewed X-inactivation, with a 96:4 distribution (Figure S3). The outcome of the X-inactivation process, measured by the androgen receptor locus, seems to be consistent within the same clone. An independent differentiation of the same clone (RTT-1155del32 C15) yielded a 98:2 distribution. Unfortunately, androgen receptor locus analysis was not conclusive for the MeCP2 mutation Q244X

differentiated populations of fibroblasts and iPSC-derived neurons have me3H3K27 nuclear foci staining, indicating X-inactivation.

We also used fluorescent in situ hybridization (FISH) to visualize Xist RNA, a noncoding transcript involved in X chromosome silencing that physically wraps the inactive X (Lucchesi et al., 2005). Before reprogramming, the majority of fibroblasts exhibit a clear Xist cloud. The signal is lost after reprogramming, indicating that selected iPSC clones have two active X chromosomes in our culture conditions. A Xist cloud is also observed in iPSC-derived neurons (Figure 3D). Fluorescent in situ hybridization (FISH) analysis using a centromeric X chromosome probe in iPSC-derived NPCs and neurons showed the presence of two X

Figure 2. Neural Differentiation of iPSCs

(A) Schematic view of the neural differentiation protocol.

(B) Representative images depicting morphological changes during neuronal differentiation. The scale bar represents 100 μm.

(C) NPCs are positive for neural precursor markers: Sox1, Sox2, Musashi1, and Nestin. The scale bar represents 50 μm.

(D–F) (D) Representative images of cells after neuronal differentiation. iPSC-derived neurons express mature neuronal markers: GABA, Map2 and Synapsin. The scale bar represents 20 μm. Similar numbers of Map2-positive and Syn::DsRed-positive (E) as well as GABA-positive (F) neurons from WT and RTT cultures.

Data shown as mean ± SEM. See also Figure S2.

Our data show that X-inactivation was erased in selected reprogrammed RTT-iPSCs clones and subsequently restored during neuronal differentiation. Importantly, the recapitulation of X-inactivation produces mosaic neuronal cultures with different ratios of cells expressing normal MeCP2 levels, mimicking what is observed in RTT patients' brains. Our data do not preclude that partial reprogramming from a single fibroblast or retention of the X-inactivation would lead to clones with highly skewed X-inactivation, where neurons would express only the normal or mutant form of MePC2. In fact, we do observe WT and RTT-iPSC clones retaining X-inactivation after reprogramming. The RTT-T158M C3-derived neurons showed 100:0 distribution. The expression of the mutant MeCP2 allele was confirmed by sequencing.

Normal Cellular Proliferation from RTT-iPSC-Derived NPCs

An increased incidence of large head size has been reported in autism (Piven et al., 1995). Other studies have suggested that the autistic brain is smaller at birth, followed by rapid head growth during early development and then a period of reduced brain growth (Courchesne et al., 2003). Head growth deceleration has also been reported for RTT patients (Hagberg et al., 2001). Since the cellular mechanism behind this phenomenon is unknown, we investigated whether a perturbed NPC replication cycle was affected in RTT. NPCs derived from RTT-iPSCs, WT-iPSCs and hESCs (Cyth25 and HUES6) were generated and kept under proliferating conditions in the presence of FGF2. NPCs were derived using the same protocol described above, had identical passage numbers and were analyzed for cell cycle by flow cytometry. Our results showed no significant differences in any cycle phase between HESC-, WT-iPSC- and RTT-iPSC-derived NPCs (Figure 4A), though we cannot exclude the possibility that

cells. However, a reduction of 50% in the amount of MeCP2 protein level (Figure S4E) is consistent with a random X-inactivation. We have not analyzed the distribution for RTT-R306C clones.

altered head growth in RTT patients is caused by eventual abnormal NPC proliferation in another developmental stage. We then investigated potential phenotypic changes in RTT neurons compared to controls.

Reduced Glutamatergic Synapse Number and Morphological Alterations in RTT Neurons

Strong evidence implicates synapse alteration in ASD, including RTT (Zoghbi, 2003). Loss of MeCP2 and doubling of MeCP2 dosage in mice have opposite effects on excitatory synapse numbers in individual neurons (Chao et al., 2007). These results suggest that MeCP2 may be a rate-limiting factor in regulating glutamatergic synapse formation and indicate that changes in excitatory synaptic strength may underlie global network alterations in RTT. Therefore, we determined whether excitatory synapse numbers were reduced in human RTT neurons. After 8 weeks of differentiation, glutamatergic neurons were identified using antibodies against VGLUT1 (Takamori et al., 2000), and dendrites were labeled with Map2 (Figure 4B). To confirm the specificity of glutamatergic neurons in our cultures, we showed that VGLUT1 puncta were mostly adjacent to the postsynaptic density-95 (Psd95) protein (Niethammer et al., 1996) (Figure S4A). We found a reduction in the density of VGLUT1 puncta from RTT-iPSCs clones carrying 3 different MeCP2 mutations compared to HUES6 and distinct WT-iPSCs-derived Map2-positive neurons, suggesting a specific defect in glutamate transport in RTT cultures (Figure 4B and Figure S4B). Since neurons carrying different MeCP2 mutations showed reduced VGLUT1 puncta in our cultures, we tested whether loss of function of MeCP2 was directly related to the number of glutamatergic synapses in our neuronal cultures. We cloned an shRNA against MeCP2 in a lentiviral vector that is able to knock-down both isoforms of MeCP2 (Figure S4C). Neurons derived from WT-iPSCs expressing the shMeCP2 showed a similar reduction in VGLUT1 puncta when compared to control neurons expressing a scramble shRNA (shControl) (Figure 4C and Figure S4B). Overexpression of MeCP2 using a lentiviral vector (Figure S4C) increased the number of VGLUT1 puncta in WT and RTT neurons (Figure 4D and Figure S4B). Our data strongly suggest that MeCP2 is a rate-limiting factor in regulating glutamatergic synapse number in human neurons.

We also investigated whether RTT neurons displayed any morphological alteration when compared to controls. To visualize neuronal anatomy, we infected the cultures with the Syn::EGFP lentivirus. Morphological analysis of RTT neurons revealed that the number of spines in RTT neurites was reduced when compared to WT neurons and after ectopic expression of shMeCP2 (Figure 4E). Consistent with this observation, the number of spines in dendrites of neurons from postmortem RTT patients' brains was previously reported to be lower than that in normal individuals (Chapleau et al., 2009). Finally, we documented that the cell soma sizes from neurons derived from the RTT-iPSCs carrying different MeCP2 mutations were smaller when compared to controls (reduction of 14.31 ± 4.83%). Similarly, loss of function using the shMeCP2 knock-down strategy in WT neurons reduced soma size at levels comparable to RTT levels (reduction of 14.52 ± 4.31%) (Figure 4F and Figure S4D).

Rescuing a RTT Neuronal Phenotype

Recent studies have shown that re-activation of MeCP2 expression knockout mice led to a prolonged life span and delayed onset or reversal of certain neurological symptoms (Giacometti et al., 2007; Guy et al., 2007). These reports suggest that some RTT phenotypes can be rescued in vivo. We used our model to analyze the effect of selected compounds that may revert the neuronal phenotype in culture as a validation for future high-throughput drug screening platforms. Administration of IGF1 was recently described to promote a partial reversal of the RTT-like symptoms in a mouse model (Tropea et al., 2009). We treated RTT-derived neurons carrying different MeCP2 mutations in culture with IGF1 and observed an increase in glutamatergic synapse number, suggesting that the drug treatment could correct the RTT neuronal phenotype (Figure 4B and Figure S4B).

Around 60% of MeCP2 mutations in RTT are nonsense mutations (Laccone et al., 2001). Thus, we tested whether we could increase MeCP2 expression levels in affected neurons by suppressing the nonsense mutation (Q244X) with read-through of the premature stop codon using pharmacological treatments. High concentrations of aminoglycosides antibiotics, such as gentamicin, can bind to the 16S rRNA, impairing ribosomal proofreading (Kellermayer, 2006). As a consequence, a full-length protein is produced by incorporating a random amino acid at the stop codon position. We treated RTT-Q244X clones 3- and 4-derived neurons with two different doses of gentamicin and found that MeCP2 protein levels and glutamatergic synapse numbers were increased after 1 week (Figure 4G and Figure S4E). Treatment with a higher gentamicin dose (400ug/ml) for the same period did not rescue RTT neurons and lowered the number of VGLUT1 puncta in control neurons (Figure 4G).

The finding that RTT patient-derived neurons displayed changes in neuronal morphology and in number of synapses prompted us to explore putative circuit alterations in vitro.

Altered Activity-Dependent Calcium Transients in RTT-iPSC-Derived Cells

Early in neural development, spontaneous electrical activity leads to increases in intracellular calcium levels and activation of signaling pathways that are important in regulating several neuronal processes (Spitzer et al., 2004). Recently, a disturbance in calcium homeostasis during early postnatal development was reported in a MeCP2 knockout model (Mironov et al., 2009). Moreover, several studies showed that functional mutations in genes encoding voltage-gated calcium channels and in genes whose activity is modulated by calcium, such as MeCP2, could lead to ASD (Splawski et al., 2006; Zhou et al., 2006). Neuronal activity-induced calcium influx can trigger the calcium/calmodulin-dependent protein kinase (CamK). CamK activation has been reported to induce phosphorylation of MeCP2, which was further postulated to regulate neuronal spine maturation (Tao et al., 2009; Zhou et al., 2006). Although these studies raised an interesting link between neuronal activity and spine maturation, the extent of cellular alteration in human ASD neurons was never characterized. To test if RTT-iPSCs-derived neuronal networks are affected in our system, we preloaded the cells with the calcium indicator fluo-4AM and highlighted neurons using
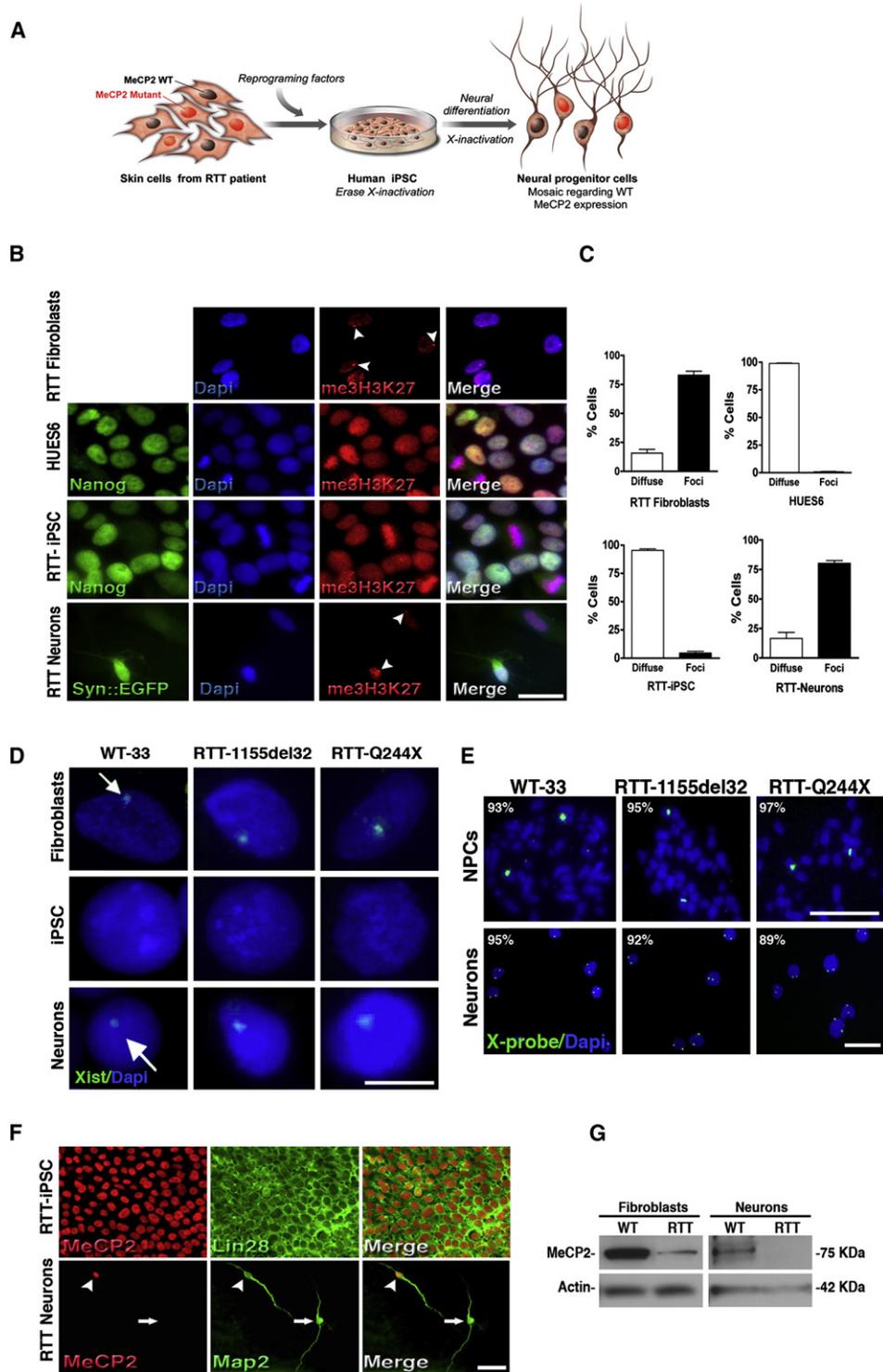
Figure 3. RTT-iPSC Clones Undergo X-Inactivation during Differentiation

(A) Schematic representation of X-inactivation dynamics during reprogramming and further neural differentiation. RTT fibroblasts are mosaic for the MeCP2 WT gene expression. During reprogramming, X-inactivation is erased and iPSCs express both MeCP2 alleles. Upon neuronal differentiation, X-inactivation is re-established and the resultant cells are mosaic for MeCP2 WT gene expression.

(B) Immunofluorescence for me3H3K27 in fibroblasts, pluripotent cells (Nanog-positive) and after neuronal differentiation (Syn::EGFP-positive). Pluripotent cells (hESCs and iPSCs) show diffuse staining whereas differentiated cells (fibroblasts and neurons) exhibit prominent me3H3K27 nuclear foci (arrowheads). Cells were counterstained with Dapi. The scale bar represents 15 μm.

the Syn::DsRed vector. Cultures with similar cell density and numbers of DsRed-positive neurons were used (Figure S2B). Spontaneous calcium transients were analyzed from WT and RTT neuronal networks in several independent experiments over time (Figure 5).

In our analyses, we only considered calcium transients generated by synaptic activity. Neurons were selected after confirmation that calcium transients were blocked with TTX or with the glutamate receptor antagonists CNQX (AMPA) and APV (NMDA) treatments, indicating neuronal signaling dependence on local synaptic connections (Figures S5A, S5B, and S5D). Gabazine, an antagonist of GABAa receptors, increased the number of calcium transients in the networks, indicating the presence of glutamatergic and gabaergic synapses in our system (Figure S5C, D). A representative example of calcium tracing in control and RTT neurons is depicted in Figure 5A and shows a sharp increase in amplitude followed by a decrease over time. The frequency of calcium oscillations in RTT neurons and in WT neurons expressing shMeCP2 was abnormally decreased when compared to controls, suggesting a deficiency in the neuronal network connectivity and activity dynamics (Figures 5B and 5C and Figures S5E and S5F). The deficiency in connectivity was further corroborated by a decrease in the percentage of Syn::DsRed-positive neurons exhibiting calcium transients in the RTT cultures when compared to controls (Figure 5D and Figure S5F).

Decreased Frequency of Spontaneous Postsynaptic Currents in RTT Neurons

Next we determined the functional maturation of the iPSC-derived neurons using electrophysiological methods. Whole-cell recordings were performed from cells that had differentiated for at least 6 weeks in culture. Neurons were visualized by infection with the Syn::EGFP viral vector (Figure 6A). Both WT and RTT neurons showed similar transient sodium inward currents, sustained potassium outward currents in response to voltage step depolarizations, and action potentials evoked by somatic current injections (Figure 6B). Therefore, our data indicated that WT and RTT reprogramming did not affect the ability of WT-iPSC- and RTT-iPSC-derived neurons to mature and become electrophysiologically active. We also recorded spontaneous excitatory and inhibitory postsynaptic currents (sEPSCs and sIPSCs) as a way of measuring intercellular connectivity and network formation (Figures 6B and 6C). Cumulative probability plots of amplitudes and inter-event intervals of spontaneous postsynaptic currents revealed that RTT neurons have a significant decrease in frequency and amplitude when compared to WT neurons (Figures 6D and 6E). Together, our data suggest that the neuronal network is altered in RTT iPSC-derived cultures.

DISCUSSION

The lack of detectable symptoms in female RTT patients until 6–18 months of age and the apparent phenotypic reversibility of some RTT phenotypes in MeCP2 knockout animals indicate that MeCP2 is not essential for early wiring of the nervous system but instead may only be required at late stages. It is possible that RTT patients have aberrant excitatory synaptic strength at very early stages, when the disease phenotype is not yet clearly observed. In fact, increasing evidence from clinical studies and mouse models indicates the presence of alterations during the so-called presymptomatic developmental phase (Charman et al., 2002; De Filippis et al., 2009; Kerr et al., 1987; Picker et al., 2006; Santos et al., 2007).

To study human RTT neurons in culture, we derived iPSCs from RTT fibroblasts. RTT iPSCs are pluripotent and able to recapitulate X-inactivation upon neuronal differentiation. Even though the ratio of neurons expressing mutant MeCP2 due to X-inactivation was variable, the phenotypes described here for all RTT-derived neurons are similar. One interpretation could be that astrocytes, or other nonneuronal cells, carrying MeCP2 mutations present in our cultures could also affect neurons expressing the normal MeCP2 protein. In fact, the non-cell-autonomous influence was recently described for RTT, indicating that glial cells carrying MeCP2 mutations can distress healthy neurons (Ballas et al., 2009; Kishi and Macklis, 2010; Maezawa et al., 2009).

Using human neurons carrying MeCP2 mutations, we showed that RTT glutamatergic neurons have a reduced number of synapses and dendritic spines when compared to nonaffected controls. Moreover, electrophysiological recordings from RTT neurons showed a significant decrease in the frequency and amplitude of spontaneous synaptic currents compared to WT neurons. The reduced frequency in RTT neurons could reflect the presence of fewer release sites or a decreased release probability. The results of electrophysiology recordings are consistent with the decreased VGLUT1 puncta observed in Map2-positive dendrites from RTT neurons. Also consistent with these findings, the frequency of intracellular calcium transients was decreased in RTT neurons when compared to controls. Our data indicate a potential imbalance in the neuronal networks associated with RTT pathology. The observations described here provide valuable information for RTT and, potentially, ASD patients, since they suggest that presymptomatic defects may represent novel biomarkers to be exploited as diagnostic tools and that early intervention may be beneficial.

Therapies aiming at earlier stages of development may attenuate the downstream consequences of MeCP2 mutations. Restoring protein levels may be challenging, since MeCP2 levels are tightly regulated and chronically overdosing neurons with the

(C) Quantification of cells with diffused or foci me3H3K27 nuclear staining. Data shown as mean ± SEM.

(D) RNA FISH shows that Xist RNA domains are present in the original fibroblasts before reprogramming. iPSCs show no Xist expression. Neurons derived from normal and RTT iPSCs show clear Xist clouds, indicating transcriptional silencing of the X chromosome (arrows). The scale bar represents 5 μm.

(E) Two DNA FISH signals are evident in the nuclei of iPSC-derived NPCs and neurons, revealing the presence of two X chromosomes. The scale bar represents 10 μm.

(F) RTT-iPSCs (1155del32) expressed WT MeCP2 but derived neurons displayed mosaicism regarding WT (arrowhead) and mutant (arrow) MeCP2 forms. The scale bar represents 50 μm.

(G) RTT-derived fibroblasts and neurons have reduced levels of WT MeCP2 protein by Western blot. See also Figure S3.
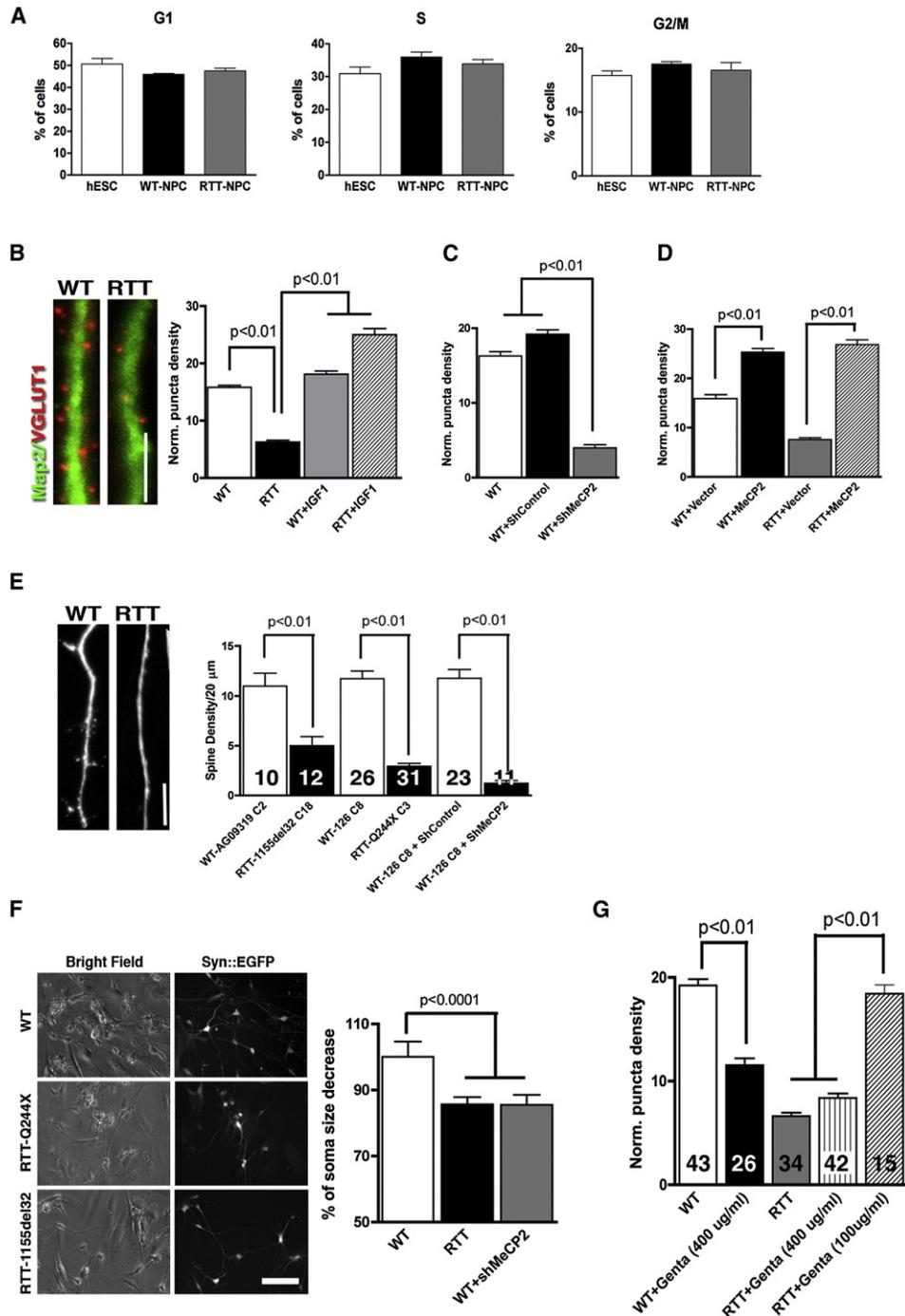
Figure 4. Alterations in RTT Neurons

(A) Proliferating RTT NPCs displayed no signal of aberrant cell cycle when compared to controls.

(B) Representative images of neurons showing VGLUT1 puncta on Map2 neurites. Bar graphs show synaptic density in RTT and WT neurons. IGF1 treatment increased VGLUT1 puncta number in RTT-derived neurons. The scale bar represents 5 μm.

(C) Reduction of MeCP2 expression decreased the number of glutamatergic synapses in WT neurons.

(D) Overexpression of MeCP2 increased the number of glutamatergic synapses.

(E) Representative images of neurites of different genetic backgrounds. Bar graph shows the spine density from independent experiments using different RTT backgrounds and controls and after expression of shMeCP2. The scale bar represents 5 μm.

(F) Representative images of neuronal cell body size. Bar graph shows the percentage of soma size decrease in RTT compared to WT neurons. Neuronal morphology was visualized using the Syn::EGFP lentiviral vector. The scale bar represents 50 μm.

(G) A lower dose of gentamicin was able to rescue glutamatergic synapses in RTT neurons. Numbers of neurons analyzed (*n*) are shown within the bars in graphs (E) and (G). For all clones and mutations used refer to Figure S4 and Table S2. Data shown as mean ± SEM.
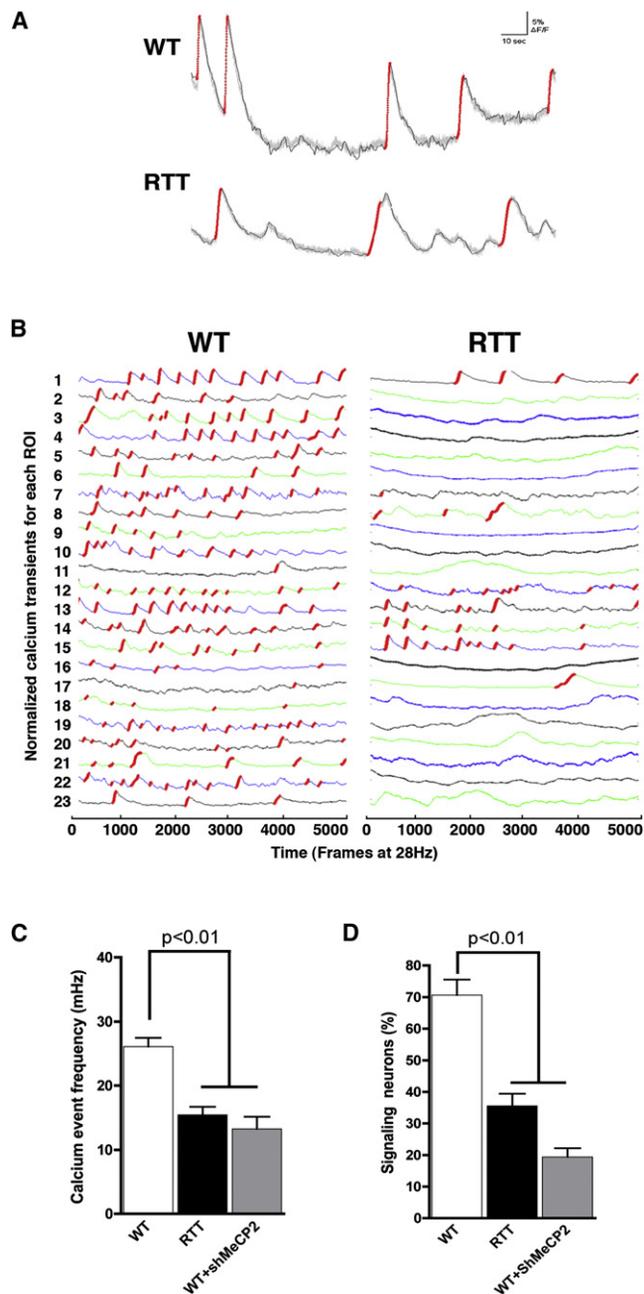
Figure 5. Altered Activity-Dependent Calcium Transients in RTT-Derived Neurons

(A) Representative examples of WT and RTT calcium signal traces. Red traces correspond to the calcium rise phase detected by the algorithm used (see Extended Experimental Procedures).

(B) Fluorescence intensity changes reflecting intracellular calcium fluctuations in RTT and WT neurons in different Regions of Interest (ROI).

(C) RTT neurons show a lower average of calcium spikes when compared to WT control neurons.

(D) The percentage of Syn::DsRed-positive neurons signaling in the RTT neuronal network is significantly reduced when compared to controls. Data shown as mean ± SEM. See also Figure S5.

WT allele can be as harmful as a loss of expression (Collins et al., 2004; Ramocki et al., 2009; Van Esch et al., 2005). Thus, we tested pharmacological treatment as a way to recover the RTT neuronal phenotype. We investigated the use of IGF1 in human neuronal cultures. Although it likely acts in a nonspecific manner, IGF1 is considered to be a candidate for pharmacological treatment of RTT and potentially other CNS disorders in a future clinical trial (Tropea et al., 2009). While IGF1 treatment increased synapse number in some clones, it stimulated glutamatergic RTT neurons above normal levels. Our data indicate that the IGF1 dose and timing parameters need to be precisely tuned in future clinical trials to avoid side effects. In a different approach, we tested a read-through drug (gentamicin) to rescue neurons derived from iPSCs carrying a nonsense MeCP2 mutation. A lower dosage of gentamicin was enough to increase full-length MeCP2 levels in RTT neurons, rescuing glutamatergic synapses. New drugs with reduced toxicity and enhanced suppression of premature stop codon mutations might be good therapeutic candidates (Nudelman et al., 2009; Welch et al., 2007).

Control of glutamatergic synapse number and the other neuronal phenotypes analyzed here may be caused by loss of MeCP2 function in the cell. Alternatively, significant experimental and genomic variability in our system could be directly responsible for the RTT differences displayed in our data. Our gain and loss of function data strongly suggest that MeCP2 is indeed the causative agent of the cellular phenotypes reported here that might be relevant to the clinical features of RTT.

Our data indicate that iPSCs not only can recapitulate some aspects of a genetic disease but also can be used to better design and anticipate results from translational medicine. This cellular model has the potential to lead to the discovery of new compounds to treat RTT and other forms of ASD. Finally, other CNS diseases may be modeled in vitro using a similar approach.

EXPERIMENTAL PROCEDURES

Cell Culture and Retrovirus Infection

Female RTT and control fibroblasts were generated from explants of dermal biopsies following informed consent under protocols approved by the University of California San Diego. The Syn::EGFP or DsRed reporter vector was obtained by cloning the Synapsin-1 promoter (a gift from Dr. G. Thiel, Hamburg, Germany) in a lentivirus backbone. The shRNA against a target sequence on the human MeCP2 gene was cloned in the LentiLox3.7 lentivirus vector. Retrovirus vectors containing the Oct4, c-Myc, Klf4 and Sox2 human cDNAs from Yamanaka's group (Takahashi et al., 2007) were obtained from Addgene. Two days after infection, fibroblasts were plated on mitotically inactivated mouse embryonic fibroblasts (Chemicon) with hESC medium. After 2 weeks, iPSC colonies were directly transferred to feeder-free conditions on matrigel-coated dishes (BD) using mTeSR1 (StemCell Technologies, and passed manually. The detailed protocols to obtain NPCs and mature neurons are described in the supplemental material. For the rescue experiments, 10 ηg/mL of IGF1 (Peprotech) or Gentamicin (Invitrogen; at 100 or 400 μg/mL) was added to neuronal cultures for 1 week. Protocols were previously approved by the University of California San Diego and Salk Institute Institutional Review Board and the Embryonic Stem Cell Research Oversight Committee.

Immunocytochemistry and Neuronal Morphology Quantification

Cells were briefly fixed in 4% paraformaldehyde and then permeabilized with 0.5% Triton X-100 in PBS. Cells were then blocked in PBS containing 0.5% Triton X-100 and 5% donkey serum for 1 hr before incubation with primary antibody overnight at 4°C. After three washes with PBS, cells were incubated
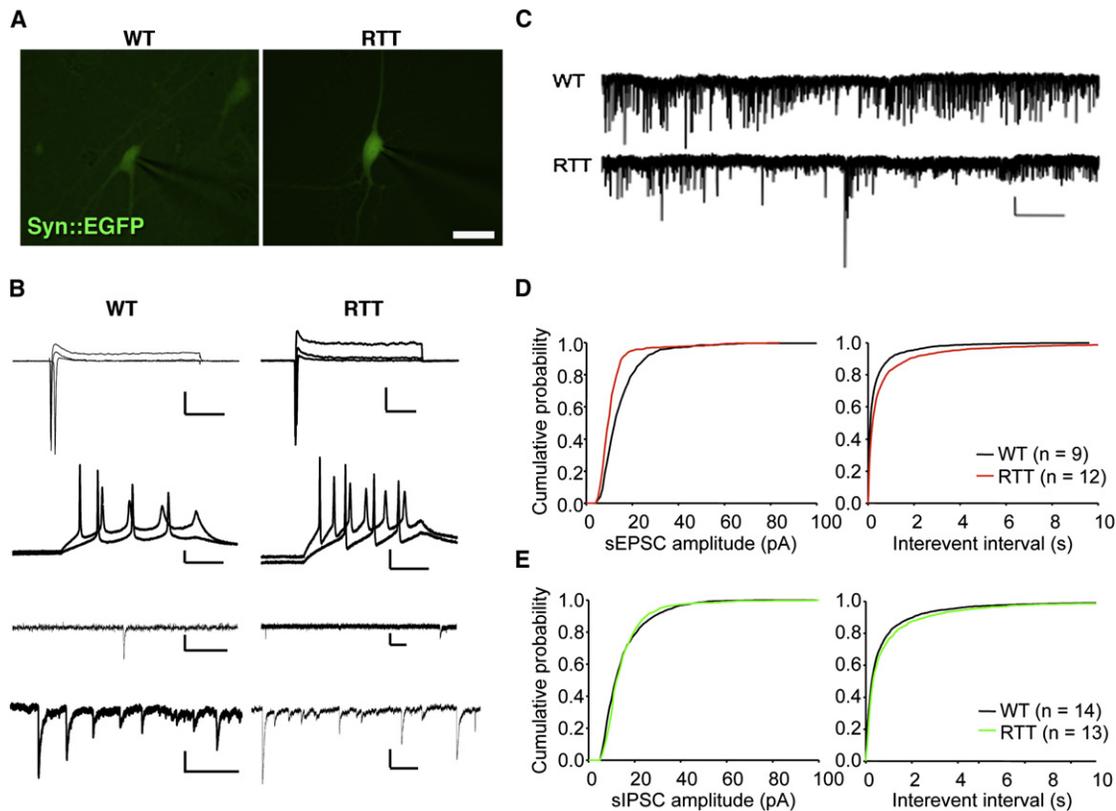
Figure 6. Decreased Frequency of Spontaneous Postsynaptic Currents in RTT Neurons

(A) Fluorescence micrographs of representative WT and RTT neurons. The scale bar represents 10 μm.

(B) Electrophysiological properties of WT and RTT neurons. From top to bottom: Transient Na^+ currents and sustained K^+ currents in response to voltage step depolarizations (command voltage varied from -20 to $+30$ mV in 5 mV increments when cells were voltage-clamped at -70 mV, Bars = 400 pA and 50 ms). Action potentials evoked by somatic current injections (cells current-clamped at around -60 mV, injected currents from 10 to 40 pA, Bars = 20 mV and 100 ms), sEPSCs (Bars = right, 20 pA, 100 ms; left: 10 pA, 500 ms), and sIPSCs (Bars = right, 20 pA, 500 ms; left: 20 pA, 400 ms).

(C) Sample 4 min recordings of spontaneous currents when the cells were voltage-clamped at -70 mV (Bars = 20 pA and 25 s).

(D) Cumulative probability plot of amplitudes (left panel, 1 pA bins; $p < 0.001$) and inter-event intervals (right panel, 20 ms bins; $p < 0.05$) of sEPSCs from groups of WT (black) and RTT (red) cells, respectively.

(E) Cumulative probability plot of amplitudes (left panel, 1 pA bins; $p < 0.05$) and inter-event intervals (right panel, 20 ms bins; $p < 0.05$) of sIPSCs from each group (WT, black; RTT, green).

with secondary antibodies (Jackson ImmunoResearch) for 1 hr at room temperature. Fluorescent signals were detected using a Zeiss inverted microscope and images were processed with Photoshop CS3 (Adobe Systems). Primary antibodies used in this study are described in the supplemental information. Cell soma size was measure in bright field using ImageJ software after identification of neurons using the Syn::EGFP. The morphologies of neuronal dendrites and spines were studied from an individual projection of z-stacks optical sections and scanned at 0.5-μm increments that correlated with the resolution valued at z-plane. Each optical section was the result of 3 scans at 500 lps followed by Kalman filtering. For synapse quantification, images were taken by a z-step of 1 μm using Biorad radiance 2100 confocal microscope. Synapse quantification was done blinded to genotype. Only VGLUT1 puncta along Map2-positive processes were counted. Statistical significances were tested using Two-way ANOVA test and Bonferroni post-test.

Cell Cycle Analysis

One million NPCs were fixed in 70% EtOH for at least 2 hr at 4°C. After PBS washing, cells were stained with 1 ml of propidium iodide (PI) solution (50 μg/mL PI in 3.8 Mm sodium citrate) and treated with 20 μL/mL of RNaseA. Cells were analyzed by fluorescence-activated cell sorting (FACS) on a Becton

Dickinson LSRI and cell cycle gating was examined using FLOWJO - Flow Cytometry Analysis Software.

RNA Extraction and RT-PCR

Total cellular RNA was extracted from ∼5×10^6 cells using the RNeasy Protect Mini kit (QIAGEN, Valencia, CA), according to the manufacturer's instructions, and reverse transcribed using the SuperScript III First-Strand Synthesis System RT-PCR from Invitrogen. The cDNA was amplified by PCR using Accuprime Taq DNA polymerase system (Invitrogen). Primer sequences used are described in Supplemental information.

Teratoma Formation in Nude Mice

Around 1-3 x10^6 fibroblasts or iPSCs were injected subcutaneously into the dorsal flanks of nude mice (CByJ.Cg-Foxn1nu/J) anesthetized with isoflurane. Five to six weeks after injection, teratomas were dissected, fixed overnight in 10% buffered formalin phosphate and embedded in paraffin. Sections were stained with hematoxylin and eosin for further analysis. Control mice injected with RTT fibroblasts failed to form teratomas. Protocols were previously approved by the University of California San Diego Institutional Animal Care and Use Committee.

Karyotyping and DNA Fingerprinting
Standard G-banding chromosome and DNA fingerprinting analysis was performed by Cell Line Genetics (Madison, WI).

DNA and RNA FISH
Xist RNA exon 6 probes (GenBank U80460: 75081-78658 – a gift from Dr. Jeannie T. Lee, Massachusetts General Hospital, Harvard Medical School) were transcribed by using T7 RNA polymerase (Roche) with AlexaFluor 488-5-UTP. X chromosome probe and Xist slide hybridization were performed by Molecular Diagnostic Services, Inc. (San Diego, CA).

Protein Isolation and Western Blot Analysis
Cells were isolated, suspended in 1× RIPA lyses buffer (Upstate) supplemented with 1% protease inhibitor cocktail (Sigma), triturated and centrifuged at 10,000 × g for 10 min at 4°C. Twenty micrograms of total protein was separated on 12% SDS-polyacrylamide gel, transferred to a nitrocellulose membrane and probed with a primary antibody against MeCP2 (1:5,000; Diagenode), followed by horseradish-peroxidase-conjugated secondary antibody (1:5,000; Promega), and then visualized using ECL chemiluminescence (Amersham). As a control, membranes were stripped and re-probed for β-actin (1:10,000; Ambion) or α–tubulin (1:5,000, Ambion). For semiquantitative analysis, MeCP2 signal intensity was analyzed and corrected with respect to β-actin.

Microarray Analysis
The Affymetrix Power Tools (APT) suite of programs and Affymetrix Human Gene 1.0 ST Arrays library files and annotation were obtained from http://www.affymetrix.com/support and details of the analysis are available in Supplemental information.

Calcium Imaging
Neuronal networks derived from human iPSCs were previously infected with the lentiviral vector carrying the Syn:DsRed reporter construct. Cell cultures were washed twice with sterile Krebs HEPES Buffer (KHB) and incubated with 2–5 μM Fluo-4AM (Molecular Probes/Invitrogen, Carlsbad, CA) in KHB for 40 min at room temperature. Excess dye was removed by washing twice with KHB and an additional 20 min incubation was done to equilibrate intracellular dye concentration and allow de-esterification. Time-lapse image sequences (100× magnification) of 5000 frames were acquired at 28 Hz with a region of 336 × 256 pixels, using a Hamamatsu ORCA-ER digital camera (Hamamatsu Photonics K.K., Japan) with a 488 nm (FITC) filter on an Olympus IX81 inverted fluorescence confocal microscope (Olympus Optical, Japan). Images were acquired with MetaMorph 7.7 (MDS Analytical Technologies, Sunnyvale, CA). Images were subsequently processed using ImageJ (http://rsbweb.nih.gov/ij/) and custom written routines in Matlab 7.2 (Mathworks, Natick, MA). Detailed quantitative analysis of calcium transients is available in the Supplemental material.

Electrophysiology
Whole-cell patch clamp recordings were performed from cells co-cultured with astrocytes after 6 weeks of differentiation. The bath was constantly perfused with fresh HEPES-buffered saline (see supplemental methods for recipe). The recording micropipettes (tip resistance 3–6 MΩ) were filled with internal solution described in the Supplemental materials. Recordings were made using Axopatch 200B amplifier (Axon Instruments). Signals were filtered at 2 kHz and sampled at 5 kHz. The whole-cell capacitance was fully compensated. The series resistance was uncompensated but monitored during the experiment by the amplitude of the capacitive current in response to a 10 mV pulse. All recordings were performed at room temperature and chemicals were purchased from Sigma. Frequency and amplitude of spontaneous postsynaptic currents were measured with the Mini Analysis Program software (Synaptosoft, Leonia, NJ). Statistical comparisons of WT and RTT groups were made using the nonparametric Kolmogorov-Smirnov two-tailed test, with a significance criterion of p = 0.05. EPSCs were blocked by CNQX or DNQX (10–20 μM) and IPSPs were inhibited by bicuculine (20 μM).

REFERENCES

Allen, R.C., Zoghbi, H.Y., Moseley, A.B., Rosenblatt, H.M., and Belmont, J.W. (1992). Methylation of HpaII and HhaI sites near the polymorphic CAG repeat in the human androgen-receptor gene correlates with X chromosome inactivation. Am. J. Hum. Genet. 51, 1229–1239.

Amir, R.E., Van den Veyver, I.B., Wan, M., Tran, C.Q., Francke, U., and Zoghbi, H.Y. (1999). Rett syndrome is caused by mutations in X-linked MECP2, encoding methyl-CpG-binding protein 2. Nat. Genet. 23, 185–188.

Autism and Developmental Disabilities Monitoring Network Surveillance Year 2000 Prinicipal Investigators; Centers for Disease Control and Prevention. (2007). Prevalence of autism spectrum disorders–autism and developmental disabilities monitoring network, six sites, United States, 2000. MMWR Surveill Summ 56, 1–11.

Ballas, N., Lioy, D.T., Grunseich, C., and Mandel, G. (2009). Non-cell autonomous influence of MeCP2-deficient glia on neuronal dendritic morphology. Nat. Neurosci. 12, 311–317.

Chahrour, M., Jung, S.Y., Shaw, C., Zhou, X., Wong, S.T., Qin, J., and Zoghbi, H.Y. (2008). MeCP2, a key contributor to neurological disease, activates and represses transcription. Science 320, 1224–1229.

Chao, H.T., Zoghbi, H.Y., and Rosenmund, C. (2007). MeCP2 controls excitatory synaptic strength by regulating glutamatergic synapse number. Neuron 56, 58–65.

Chapleau, C.A., Calfa, G.D., Lane, M.C., Albertson, A.J., Larimore, J.L., Kudo, S., Armstrong, D.L., Percy, A.K., and Pozzo-Miller, L. (2009). Dendritic spine pathologies in hippocampal pyramidal neurons from Rett syndrome brain and after expression of Rett-associated MECP2 mutations. Neurobiol. Dis. 35, 219–233.

Charman, T., Cass, H., Owen, L., Wigram, T., Slonims, V., Weeks, L., Wisbeach, A., and Reilly, S. (2002). Regression in individuals with Rett syndrome. Brain Dev. 24, 281–283.

Collins, A.L., Levenson, J.M., Vilaythong, A.P., Richman, R., Armstrong, D.L., Noebels, J.L., David Sweatt, J., and Zoghbi, H.Y. (2004). Mild overexpression of MeCP2 causes a progressive neurological disorder in mice. Hum. Mol. Genet. 13, 2679–2689.

Courchesne, E., Carper, R., and Akshoomoff, N. (2003). Evidence of brain overgrowth in the first year of life in autism. JAMA 290, 337–344.

De Filippis, B., Ricceri, L., and Laviola, G. (2009). Early postnatal behavioral changes in the Mecp2-308 truncation mouse model of Rett syndrome. Genes Brain Behav. 9, 213–223.

Dhara, S.K., and Benvenisty, N. (2004). Gene trap as a tool for genome annotation and analysis of X chromosome inactivation in human embryonic stem cells. Nucleic Acids Res. 32, 3995–4002.

Dimos, J.T., Rodolfa, K.T., Niakan, K.K., Weisenthal, L.M., Mitsumoto, H., Chung, W., Croft, G.F., Saphier, G., Leibel, R., Goland, R., et al. (2008). Induced pluripotent stem cells generated from patients with ALS can be differentiated into motor neurons. Science 321, 1218–1221.

Ebert, A.D., Yu, J., Rose, F.F., Jr., Mattis, V.B., Lorson, C.L., Thomson, J.A., and Svendsen, C.N. (2009). Induced pluripotent stem cells from a spinal muscular atrophy patient. Nature 457, 277–280.

Giacometti, E., Luikenhuis, S., Beard, C., and Jaenisch, R. (2007). Partial rescue of MeCP2 deficiency by postnatal activation of MeCP2. Proc. Natl. Acad. Sci. USA 104, 1931–1936.

Guy, J., Gan, J., Selfridge, J., Cobb, S., and Bird, A. (2007). Reversal of neurological defects in a mouse model of Rett syndrome. Science 315, 1143–1147.

Hagberg, G., Stenbom, Y., and Engerström, I.W. (2001). Head growth in Rett syndrome. Brain Dev. 23 (Suppl 1), S227–S229.

Hammer, S., Dorrani, N., Dragich, J., Kudo, S., and Schanen, C. (2002). The phenotypic consequences of MECP2 mutations extend beyond Rett syndrome. Ment. Retard. Dev. Disabil. Res. Rev. 8, 94–98.

Hotta, A., Cheung, A.Y., Farra, N., Vijayaragavan, K., Séguin, C.A., Draper, J.S., Pasceri, P., Maksakova, I.A., Mager, D.L., Rossant, J., et al. (2009). Isolation of human iPS cells using EOS lentiviral vectors to select for pluripotency. Nat. Methods 6, 370–376.

Kellermayer, R. (2006). Translational readthrough induction of pathogenic nonsense mutations. Eur. J. Med. Genet. 49, 445–450.

Kerr, A.M., Montague, J., and Stephenson, J.B. (1987). The hands, and the mind, pre- and post-regression, in Rett syndrome. Brain Dev. 9, 487–490.

Kishi, N., and Macklis, J.D. (2010). MeCP2 functions largely cell-autonomously, but also non-cell-autonomously, in neuronal maturation and dendritic arborization of cortical pyramidal neurons. Exp. Neurol. 222, 51–58.

Laccone, F., Huppke, P., Hanefeld, F., and Meins, M. (2001). Mutation spectrum in patients with Rett syndrome in the German population: Evidence of hot spot regions. Hum. Mutat. 17, 183–190.

Lee, G., Papapetrou, E.P., Kim, H., Chambers, S.M., Tomishima, M.J., Fasano, C.A., Ganat, Y.M., Menon, J., Shimizu, F., Viale, A., et al. (2009). Modelling pathogenesis and treatment of familial dysautonomia using patient-specific iPSCs. Nature 461, 402–406.

Lucchesi, J.C., Kelly, W.G., and Panning, B. (2005). Chromatin remodeling in dosage compensation. Annu. Rev. Genet. 39, 615–651.

Maezawa, I., Swanberg, S., Harvey, D., LaSalle, J.M., and Jin, L.W. (2009). Rett syndrome astrocytes are abnormal and spread MeCP2 deficiency through gap junctions. J. Neurosci. 29, 5051–5061.

Maherali, N., Sridharan, R., Xie, W., Utikal, J., Eminli, S., Arnold, K., Stadtfeld, M., Yachechko, R., Tchieu, J., Jaenisch, R., et al. (2007). Directly reprogrammed fibroblasts show global epigenetic remodeling and widespread tissue contribution. Cell Stem Cell 1, 55–70.

Marchetto, M.C., Winner, B., and Gage, F.H. (2010). Pluripotent stem cells in neurodegenerative and neurodevelopmental diseases. Hum. Mol. Genet. 19 (R1), R71–R76.

Mironov, S.L., Skorova, E., Hartelt, N., Mironova, L.A., Hasan, M.T., and Kügler, S. (2009). Remodelling of the respiratory network in a mouse model of Rett syndrome depends on brain-derived neurotrophic factor regulated slow calcium buffering. J. Physiol. 587, 2473–2485.

Muotri, A.R. (2008). Modeling epilepsy with pluripotent human cells. Epilepsy Behav. 14 (Suppl.), 81–85.

Niethammer, M., Kim, E., and Sheng, M. (1996). Interaction between the C terminus of NMDA receptor subunits and multiple members of the PSD-95 family of membrane-associated guanylate kinases. J. Neurosci. 16, 2157–2163.

Nudelman, I., Rebibo-Sabbah, A., Cherniavsky, M., Belakhov, V., Hainrichson, M., Chen, F., Schacht, J., Pilch, D.S., Ben-Yosef, T., and Baasov, T. (2009).

Development of novel aminoglycoside (NB54) with reduced toxicity and enhanced suppression of disease-causing premature stop mutations. J. Med. Chem. 52, 2836–2845.

Park, I.H., Arora, N., Huo, H., Maherali, N., Ahfeldt, T., Shimamura, A., Lensch, M.W., Cowan, C., Hochedlinger, K., and Daley, G.Q. (2008). Disease-specific induced pluripotent stem cells. Cell 134, 877–886.

Picker, J.D., Yang, R., Ricceri, L., and Berger-Sweeney, J. (2006). An altered neonatal behavioral phenotype in Mecp2 mutant mice. Neuroreport 17, 541–544.

Piven, J., Arndt, S., Bailey, J., Havercamp, S., Andreasen, N.C., and Palmer, P. (1995). An MRI study of brain size in autism. Am. J. Psychiatry 152, 1145–1149.

Piven, J., Palmer, P., Jacobi, D., Childress, D., and Arndt, S. (1997). Broader autism phenotype: evidence from a family history study of multiple-incidence autism families. Am. J. Psychiatry 154, 185–190.

Ramocki, M.B., Peters, S.U., Tavyev, Y.J., Zhang, F., Carvalho, C.M., Schaaf, C.P., Richman, R., Fang, P., Glaze, D.G., Lupski, J.R., and Zoghbi, H.Y. (2009). Autism and other neuropsychiatric symptoms are prevalent in individuals with MeCP2 duplication syndrome. Ann. Neurol. 66, 771–782.

Ronald, A., Happé, F., Bolton, P., Butcher, L.M., Price, T.S., Wheelwright, S., Baron-Cohen, S., and Plomin, R. (2006). Genetic heterogeneity between the three components of the autism spectrum: a twin study. J. Am. Acad. Child Adolesc. Psychiatry 45, 691–699.

Samaco, R.C., Hogart, A., and LaSalle, J.M. (2005). Epigenetic overlap in autism-spectrum neurodevelopmental disorders: MECP2 deficiency causes reduced expression of UBE3A and GABRB3. Hum. Mol. Genet. 14, 483–492.

Samaco, R.C., Nagarajan, R.P., Braunschweig, D., and LaSalle, J.M. (2004). Multiple pathways regulate MeCP2 expression in normal brain development and exhibit defects in autism-spectrum disorders. Hum. Mol. Genet. 13, 629–639.

Santos, M., Silva-Fernandes, A., Oliveira, P., Sousa, N., and Maciel, P. (2007). Evidence for abnormal early development in a mouse model of Rett syndrome. Genes Brain Behav. 6, 277–286.

Silva, J., Mak, W., Zvetkova, I., Appanah, R., Nesterova, T.B., Webster, Z., Peters, A.H., Jenuwein, T., Otte, A.P., and Brockdorff, N. (2003). Establishment of histone h3 methylation on the inactive X chromosome requires transient recruitment of Eed-Enx1 polycomb group complexes. Dev. Cell 4, 481–495.

Soldner, F., Hockemeyer, D., Beard, C., Gao, Q., Bell, G.W., Cook, E.G., Hargus, G., Blak, A., Cooper, O., Mitalipova, M., et al. (2009). Parkinson's disease patient-derived induced pluripotent stem cells free of viral reprogramming factors. Cell 136, 964–977.

Spitzer, N.C., Root, C.M., and Borodinsky, L.N. (2004). Orchestrating neuronal differentiation: patterns of Ca2+ spikes specify transmitter choice. Trends Neurosci. 27, 415–421.

Splawski, I., Yoo, D.S., Stotz, S.C., Cherry, A., Clapham, D.E., and Keating, M.T. (2006). CACNA1H mutations in autism spectrum disorders. J. Biol. Chem. 281, 22085–22091.

Takahashi, K., Tanabe, K., Ohnuki, M., Narita, M., Ichisaka, T., Tomoda, K., and Yamanaka, S. (2007). Induction of pluripotent stem cells from adult human fibroblasts by defined factors. Cell 131, 861–872.

Takahashi, K., and Yamanaka, S. (2006). Induction of pluripotent stem cells from mouse embryonic and adult fibroblast cultures by defined factors. Cell 126, 663–676.

Takamori, S., Rhee, J.S., Rosenmund, C., and Jahn, R. (2000). Identification of a vesicular glutamate transporter that defines a glutamatergic phenotype in neurons. Nature 407, 189–194.

Tao, J., Hu, K., Chang, Q., Wu, H., Sherman, N.E., Martinowich, K., Klose, R.J., Schanen, C., Jaenisch, R., Wang, W., and Sun, Y.E. (2009). Phosphorylation of MeCP2 at Serine 80 regulates its chromatin association and neurological function. Proc. Natl. Acad. Sci. USA 106, 4882–4887.

Thomson, J.A., Itskovitz-Eldor, J., Shapiro, S.S., Waknitz, M.A., Swiergiel, J.J., Marshall, V.S., and Jones, J.M. (1998). Embryonic stem cell lines derived from human blastocysts. Science 282, 1145–1147.

Traynor, J., Agarwal, P., Lazzeroni, L., and Francke, U. (2002). Gene expression patterns vary in clonal cell cultures from Rett syndrome females with eight different MECP2 mutations. BMC Med. Genet. *3*, 12.

Tropea, D., Giacometti, E., Wilson, N.R., Beard, C., McCurry, C., Fu, D.D., Flannery, R., Jaenisch, R., and Sur, M. (2009). Partial reversal of Rett Syndrome-like symptoms in MeCP2 mutant mice. Proc. Natl. Acad. Sci. USA *106*, 2029–2034.

Van Esch, H., Bauters, M., Ignatius, J., Jansen, M., Raynaud, M., Hollanders, K., Lugtenberg, D., Bienvenu, T., Jensen, L.R., Gecz, J., et al. (2005). Duplication of the MECP2 region is a frequent cause of severe mental retardation and progressive neurological symptoms in males. Am. J. Hum. Genet. *77*, 442–453.

Welch, E.M., Barton, E.R., Zhuo, J., Tomizawa, Y., Friesen, W.J., Trifillis, P., Paushkin, S., Patel, M., Trotta, C.R., Hwang, S., et al. (2007). PTC124 targets genetic disorders caused by nonsense mutations. Nature *447*, 87–91.

Yasui, D.H., Peddada, S., Bieda, M.C., Vallero, R.O., Hogart, A., Nagarajan, R.P., Thatcher, K.N., Farnham, P.J., and Lasalle, J.M. (2007). Integrated epige-nomic analyses of neuronal MeCP2 reveal a role for long-range interaction with active genes. Proc. Natl. Acad. Sci. USA *104*, 19416–19421.

Yu, J., Vodyanik, M.A., Smuga-Otto, K., Antosiewicz-Bourget, J., Frane, J.L., Tian, S., Nie, J., Jonsdottir, G.A., Ruotti, V., Stewart, R., et al. (2007). Induced pluripotent stem cell lines derived from human somatic cells. Science *318*, 1917–1920.

Zappella, M., Meloni, I., Longo, I., Canitano, R., Hayek, G., Rosaia, L., Mari, F., and Renieri, A. (2003). Study of MECP2 gene in Rett syndrome variants and autistic girls. Am. J. Med. Genet. B. Neuropsychiatr. Genet. *119*, 102–107.

Zhou, Z., Hong, E.J., Cohen, S., Zhao, W.N., Ho, H.Y., Schmidt, L., Chen, W.G., Lin, Y., Savner, E., Griffith, E.C., et al. (2006). Brain-specific phosphorylation of MeCP2 regulates activity-dependent Bdnf transcription, dendritic growth, and spine maturation. Neuron *52*, 255–269.

Zoghbi, H.Y. (2003). Postnatal neurodevelopmental disorders: meeting at the synapse? Science *302*, 826–830.